Proceedings of DSCC2008
2008 ASME Dynamic Systems and Control Conference
October 20-22, 2008, Ann Arbor, Michigan, USA

DSCC2008-2155

ON CONTROLLABILITY AND OBSERVABILITY OF LINEARIZED LIQUID WATER DISTRIBUTIONS INSIDE A PEM FUEL CELL

Buz A. McCain
Fuel Cell Control Laboratory
Dept. of Mechanical Engineering
University of Michigan
Ann Arbor, Michigan 48103
Email: bmccain@umich.edu

Anna G. Stefanopoulou
Fuel Cell Control Laboratory
Dept. of Mechanical Engineering
University of Michigan
Ann Arbor, Michigan 48103

Kenneth R. Butts
Toyota Motor Engineering
and Manufacturing
Ann Arbor, Michigan 48105

ABSTRACT

We analyze the controllability and observability (C/O) of first principles-based numeric and reduced semi-analytic PEMFC models, with emphasis on the effects of model reduction on these analyses. The numeric model is a partial differential equation (PDE) based model approximated by difference equations, including both channels and both GDL of a PEMFC. The reduced model uses a semi-analytic solution (SAS) method, which is a combination of analytic and numeric solutions, gaining physical intuition at lower computational cost. The C/O analysis is based on linearizations around multiple operating points of the numeric and the semi-analytic models. The results indicate that stabilizability of the anode water states is possible.

1 INTRODUCTION AND MOTIVATION

The quantity of water within a polymer electrolyte membrane fuel cell (PEMFC) directly affects its performance, efficiency, and durability. High membrane humidity is desirable for proton conductivity, yet excess liquid water in the anode has been experimentally shown to be a cause of output voltage degradation. Liquid water occupies pore space in the gas diffusion layer (GDL), impedes the diffusion of reactant flow towards the membrane, and ultimately reduces the active fuel cell area, causing performance degradation. While it is generally understood that hydrophobicity of the GDL porous media facilitates liquid transport from GDL to channel, the interaction between GDL and channel liquid water has yet to be addressed from a controls perspective. This is a critical step for establishment of algorithms to control liquid water within the fuel cell.

The model from [1] describing the multi-component (reactants, water), two-phase (vapor and liquid water), spatially-distributed, dynamic behavior across the GDL (Fig. 1) is employed to study C/O for fuel cell water management. The time-varying constituent distributions in the GDL of each electrode are described by three second-order parabolic PDEs for reactant (oxygen in the cathode and hydrogen in the anode) concentration, water vapor concentration, and liquid water volume. The electrochemical reactions on, and the mass transport through, the catalyst-covered membrane couple the anode and cathode behaviors and, together with the channel conditions, provide the time-varying boundary values for these PDEs.

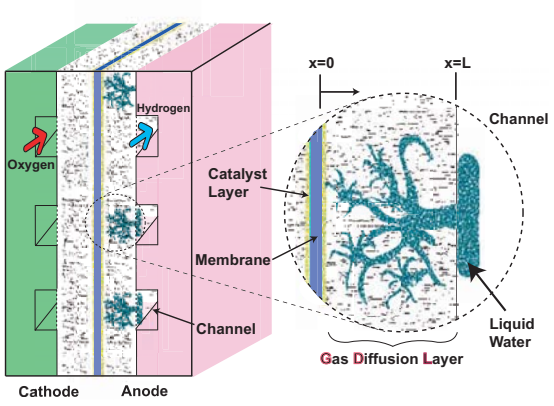

Figure 1. CONCEPTUAL SCHEMATIC SHOWING ACCUMULATION OF LIQUID WATER IN THE GDL AND SUBSEQUENT FLOW TO THE CHANNEL TO FORM REACTANT-BLOCKING FILM.

The water (liquid and vapor) PDEs are coupled through the evaporation/condensation rate. Liquid water occupies pore space in the GDL, impedes the diffusion of reactant flow towards the

membrane, and ultimately reduces the fuel cell active area [2], causing performance degradation. Removal of accumulated liquid water is necessary to regain performance, and is typically accomplished by surging an inlet flow (e.g. anode H_2 supply).

A C/O analysis based on linearization around different operating points shows that it is mathematically possible to control the GDL channel boundary conditions (BC) which is critical for stabilization of the liquid water flooding in the anode channels. It is demonstrated that the degree of coupling is affected by the operating point. For example, greater controllability of the liquid water modes is obtained when the channel condition is subsaturated than when it is saturated. On the other hand, during anode flooding (which is associated with channel vapor saturation), the GDL anode liquid water becomes uncontrollable, yet observability is gained using cell voltage output.

2 FUEL CELL MODEL

Due to space limitations, only a summary of the first principles model for the anode will be provided here. The details of the model are identical to those presented in [1], and validation of the model can be found in [3].

We proceed with a one-dimensional treatment focusing on the anode, using the following assumptions:

1. The model is spatially isothermal;
2. Convective flow of the gases in the GDL is neglected;
3. Mass transport is in 1D, normal to the membrane;
4. Water transport out of the anode channel is in vapor form.

We designate x as the spatial variable, with x=0 corresponding to the membrane location and x=L corresponding to the anode channel location, and we let t denote time.

The state variables are as follows:

1. $c_{H_2}(x,t)$ is the hydrogen concentration (mol/m^3) at time t at a cross-section of the GDL located at x, $0 \le x \le L$;
2. $c_{v,an}(x,t)$ is the concentration of water vapor at time t at a cross-section of GDL located at x, $0 \le x \le L$;
3. $s(x,t)$ is the fraction of liquid water volume V_L to the total pore volume V_p, $s = \frac{V_L}{V_p}$. s is thus a concentration-like variable for the liquid water at time t, at a cross-section of GDL located at x, $0 \le x \le L$.

A useful variable, $S(x,t)$ is the reduced water saturation at time t at a cross-section of the GDL located at x, $0 \le x \le L$,

$$S(x,t) \triangleq \begin{cases} \frac{s(x,t)-s_{im}}{1-s_{im}} & \text{for } s(x,t) \ge s_{im}, \\ 0 & \text{for } s(x,t) < s_{im}. \end{cases} \quad (1)$$

The condensed liquid accumulates in the GDL until the liquid water ratio surpasses the immobile saturation (s_{im}), at which point capillary flow will carry it to an area of lower capillary pressure (toward the GDL-channel interface). Taken from [4], the value chosen for the immobile saturation is s_{im}=0.1.

Taken from [4], and simplified in [1], the molar fluxes are driven entirely by the presence of a concentration gradient (i.e. diffusion), since bulk flow (convection) is neglected:

$$N_{H_2} = -D_{H_2}(s)\frac{\partial c_{H_2}}{\partial x}, \qquad N_v = -D_v(s)\frac{\partial c_{v,an}}{\partial x}, \quad (2)$$

where $D_v(s)$ and $D_{H_2}(s)$ are the effective diffusivities for water vapor and hydrogen which depend on the water saturation, s,

$$D_j(s) = D_{\varepsilon,j}(1-s)^2 \approx D_{\varepsilon,j}(1-s_{im})^2 \triangleq D_v^{s_{im}}, \quad (3)$$

where $D_{\varepsilon,j}$ is a constant that depends on GDL porosity (ε).

2.1 Gas Diffusion Layer Model

The gas constituent conservation equations are,

$$\frac{\partial c_{H_2}}{\partial t} = -\frac{\partial N_{H_2}}{\partial x}, \qquad \frac{\partial c_{v,an}}{\partial t} = -\frac{\partial N_v}{\partial x} + r_v(c_{v,an}), \quad (4)$$

where r_v is the evaporation rate defined as,

$$r_v(c_{v,an}) = \begin{cases} \gamma(c_v^{sat} - c_{v,an}) & \text{for } s > 0, \\ \min\{0, \gamma(c_v^{sat} - c_{v,an})\} & \text{for } s = 0 \end{cases}$$

where γ is the volumetric condensation coefficient and c_v^{sat} is the vapor saturation concentration. Note that evaporation can only occur if there is liquid water ($s > 0$) in the GDL.

The flow of liquid water is driven by the capillary pressure (p_c) gradient due to accumulation of liquid water in the GDL,

$$W_l = -\varepsilon A_{fc}\rho\frac{KK_{rl}}{\mu_l}\frac{\partial p_c}{\partial x}, \quad (5)$$

where μ_l (kg/ms) is the liquid viscosity, A_{fc} (m^2) is the fuel cell active area, K is the material-dependent absolute permeability (m^2), and the relative liquid permeability is $K_{rl} = S^3$. The capillary pressure p_c (Pa) is a fitted third-order polynomial in $S(x,t)$, the liquid water saturation,

$$p_c = \beta_{pc}\left(1.417S - 2.12S^2 + 1.263S^3\right), \quad (6)$$

where β_{pc} is a function of surface tension, absolute permeability, viscosity, and porosity [4].

To facilitate analysis, (5) is rewritten as,

$$W_l = -\varepsilon A_{fc}\rho_l\frac{K}{\mu_l}S^3\frac{dp_c}{dS}\frac{dS}{dx} \approx -\varepsilon A_{fc}\rho_l b_1 S^{b_2}\frac{dS}{dx}, \quad (7)$$

using an approximation $\frac{K}{\mu_l}S^3\frac{dp_c}{dS} \approx b_1 S^{b_2}$, where b_1 and b_2 are fitted parameters.

Conservation of liquid mass is employed to determine the rate of liquid accumulation,

$$\frac{\partial s}{\partial t} = -\frac{1}{\varepsilon A_{fc}\rho_l}\frac{\partial W_l}{\partial x} - \frac{M_v}{\rho_l}r_v(c_{v,an}), \quad (8)$$

where M_j is the molar mass of constituent j.

Combining (2) with (4) provides the two second-order parabolic PDEs that govern the anode reactant and water vapor concentrations,

$$\frac{\partial c_{H_2}}{\partial t} = \frac{\partial}{\partial x}\left(D_{H_2}^{s_{im}} \frac{\partial c_{H_2}}{\partial x}\right), \tag{9}$$

and

$$\frac{\partial c_{v,an}}{\partial t} = \frac{\partial}{\partial x}\left(D_v^{s_{im}} \frac{\partial c_{v,an}}{\partial x}\right) + r_v(c_{v,an}). \tag{10}$$

A similar result is found from (7) and (8) for s,

$$\frac{\partial s}{\partial t} = \frac{\partial}{\partial x}\left(b_1 S^{b_2} \frac{\partial S}{\partial x}\right) - \frac{M_v}{\rho_l} r_v(c_{v,an}). \tag{11}$$

2.2 Boundary Conditions

For $c_{H_2}(x,t)$, mixed Neumann-Dirichlet type boundary conditions are imposed. The channel (ch) BC is,

$$c_{H_2}|_{x=L} = c_{H_2}^{ch} = p_{H_2}^{ch}/(\mathcal{R}T), \tag{12}$$

where $\mathcal{R}$ is the universal gas constant, T is the temperature, and the anode channel hydrogen partial pressure, $p_{H_2}^{ch}$, depends on the control, $\bar{u}$, as discussed in Sec. 2.3. The membrane (mb) BC is,

$$\left.\frac{\partial c_{H_2}}{\partial x}\right|_{x=0} = -\frac{1}{D_{H_2}^{s_{im}}|_{x=0}} \cdot \frac{i(t)}{2F} = -\frac{N_{H_2}^{rct}}{D_{H_2}^{s_{im}}|_{x=0}}, \tag{13}$$

where rct indicates the reaction of H_2 at the anode catalyst, which depends on current density i, and F is Faraday's constant.

For $c_{v,e}(x,t)$, similar mixed BC are imposed ($e = an, ca$):

$$c_{v,e}|_{x=L} = c_{v,e}^{ch} = p_{v,e}^{ch}/(\mathcal{R}T), \tag{14}$$

$$\left.\frac{\partial c_{v,an}}{\partial x}\right|_{x=0} = \frac{-N^{mb}}{D_v^{s_{im}}} \qquad \left.\frac{\partial c_{v,ca}}{\partial x}\right|_{x=0} = \frac{N_v^{rct} - N^{mb}}{D_v^{s_{im}}}, \tag{15}$$

where $N_v^{rct} = \frac{i}{2F}$ is from the formation of H_2O at the cathode catalyst and the membrane water molar flux N^{mb} is governed by electro-osmotic drag and back diffusion, which are driven by current density $i(t)$ (A/m^2) and the gradient in $c_{v,e}$ across the membrane, respectively. The model for N^{mb} used here is from [2].

Finally, for the liquid water PDE, mixed BC are again imposed. Specifically, since water passing into the GDL from the membrane is in vapor form due to the assumed presence of a micro-porous barrier layer,

$$\left.\frac{\partial S}{\partial x}\right|_{x=0} = 0. \tag{16}$$

Due to the hydrophobicity of the GDL material, it is assumed that the liquid water at the channel will take a small, nonzero, value. In [5] it is shown that control of the channel water mass to a constant results in a stable GDL water distribution, thus the channel liquid boundary condition is assumed to be

$$S(L,t) = constant \geq 0. \tag{17}$$

2.3 Anode Channel Equations

For the anode channel, the governing equations for hydrogen and water are:

$$\begin{aligned} dm_{H_2}^{ch}/dt &= W_{H_2}^{in} - W_{H_2}^{out} + W_{H2}^{GDL}, \\ dm_w^{ch}/dt &= W_w^{GDL} - (W_v^{out} - W_v^{in}). \end{aligned} \tag{18}$$

For generally humidified anode inlet flow, with relative humidity (RH^{in}) and prescribed inlet flow rate ($W_{H_2}^{in}$), the inlet water mass flow rate is,

$$W_v^{in} = \frac{P_v^{in}}{P_{H_2}^{in}} \frac{M_v}{M_{H_2}} W_{H_2}^{in} \tag{19}$$

where $P_v^{in} = RH^{in} P^{sat}$, and $P_{H_2}^{in}$ is the pressure of the dry inlet gas.

The H_2 and water vapor partial pressures, which represent the channel side GDL BC, are calculated from:

$$\begin{aligned} p_{H_2}^{ch} &= \tfrac{m_{H_2}^{ch} \mathcal{R} T}{M_{H_2} V_{an}^{ch}}, \\ p_v^{ch} &= \min\left\{\tfrac{m_v^{ch} \mathcal{R} T}{M_v V^{ch}}, p_v^{sat}\right\}, \\ p^{ch} &= p_{H_2}^{ch} + p_v^{ch}. \end{aligned} \tag{20}$$

The anode exit flow rate to the ambient (amb) is modeled as a linearly proportional nozzle equation,

$$W^{out} = \bar{u} \cdot k^{out}(p^{ch} - p^{amb}), \tag{21}$$

where k^{out} is an experimentally determined nozzle orifice constant and $\bar{u}$ is a controllable valve flow $0 \leq \bar{u} \leq 1$ to remove accumulated channel water and, unfortunately, hydrogen,

$$\begin{aligned} W_{H_2}^{out} &= \frac{m_{H_2}^{ch}}{m^{ch}} W^{out}, \\ W_v^{out} &= W^{out} - W_{H_2}^{out}, \end{aligned} \tag{22}$$

where $m^{ch} = m_{H_2}^{ch} + p_v^{ch} V^{ch} M_v/(\mathcal{R}T)$.

The hydrogen and water mass flow rate from the GDL to the channel are calculated using:

$$\begin{aligned} W_{H_2}^{GDL} &= -\varepsilon A_{fc} M_{H_2} \left(D_{H_2}^{s_{im}} \frac{\partial c_{H_2}}{\partial x}\right)\Bigg|_{x=L}, \\ W_w^{GDL} &= -\varepsilon A_{fc} \left(\rho_l b_1 S^{b_2} \frac{\partial S}{\partial x} + M_v D_v^{s_{im}} \frac{\partial c_v}{\partial x}\right)\Bigg|_{x=L}. \end{aligned} \tag{23}$$

3 THE SEMI-ANALYTIC SOLUTIONS MODEL

The Semi-Analytic Solution model from [1] and [5] is summarized here for reference.

3.1 The Water Vapor Solution

The steady-state solutions implemented for the cathode and anode GDL water vapor distributions are,

$$c_{v,an}(x,t) = \alpha_1 e^{\beta x} + \alpha_2 e^{-\beta x} + c_v^{sat}, \tag{24}$$

$$c_{v,ca}(x,t) = \nu_1 e^{\beta x} + \nu_2 e^{-\beta x} + c_v^{sat}, \tag{25}$$

where

$$\beta = \sqrt{\gamma / D_v^{s_{im}}}. \tag{26}$$

The α_i are functions of the membrane water vapor transport (N^{mb}) and the anode channel condition,

$$\alpha_1 e^{\beta L} + \alpha_2 e^{-\beta L} = c_{v,an}^{ch} - c_v^{sat}, \qquad (27)$$
$$\alpha_1 - \alpha_2 = -N^{mb}/\beta D_v^{sim}.$$

Determination of N^{mb} requires knowledge of the water vapor concentrations on both sides of the membrane, which are found from

$$c_{v,an}^{mb} = (\alpha_1 + \alpha_2) + c_v^{sat}, \qquad (28)$$
$$c_{v,ca}^{mb} = (\nu_1 + \nu_2) + c_v^{sat},$$

where the *mb* signifies the value is taken at the membrane (x=0). The ν_i, similar to the α_i, are dependent upon N^{mb} and the cathode channel condition, but are additionally influenced by the water vapor reaction term N_v^{rct},

$$\nu_1 e^{-\beta L} + \nu_2 e^{\beta L} = c_{v,ca}^{ch} - c_v^{sat} \qquad (29)$$
$$\nu_1 - \nu_2 = (-N^{mb} + N_v^{rct})/\beta D_v^{sim}.$$

3.2 Liquid Water Governing Equation

An alternate form of the liquid water distribution in the porous medium is obtained by replacing the $c_{v,an}(x,t)$ coupling term in (11) by its steady-state solution (24) (the time constant of the water vapor has been show to be multiple orders of magnitude faster than that of the liquid water). Thus for $s \geq s_{im}$,

$$\frac{\partial s}{\partial t} = \frac{\partial}{\partial x}\left(b_1 S^{b_2}\frac{\partial S}{\partial x}\right) + \frac{M_v \gamma}{\rho_l}(\alpha_1 e^{\beta x} + \alpha_2 e^{-\beta x}), \qquad (30)$$

and for $0 < s < s_{im}$

$$\frac{\partial s}{\partial t} = \frac{M_v \gamma}{\rho_l}(\alpha_1 e^{\beta x} + \alpha_2 e^{-\beta x}). \qquad (31)$$

Figure 2 demonstrates that the steady-state solutions to the water PDEs lead to an exponential form for the vapor and a fractional power polynomial for the liquid. As shown in the figure, variation in the water vapor channel-side BC affects the liquid water distribution in addition to the obvious influence on the water vapor. When the channel water vapor is at saturation (dash-dot line in Fig. 2), the anode GDL-channel liquid water flow is high, and flooding occurs. Lowering the channel water vapor to c_v^{ch*}, the distributions change to the solid line, and liquid accumulation stops because GDL-channel flow ceases. Continuous channel water vapor conditions below c_v^{ch*} result in movement of the two-phase water (liquid and vapor) front from $x_{fr} = L$ to an equilibrium point within the GDL $x_{fr} < L$ (dashed line). Derivation, analysis, and discussion of the mobile front model and related mass transport claims is addressed in [3].

4 CONTROLLABILITY/OBSERVABILITY

In [2], the six 2^{nd}-order PDEs describing reactant and water dynamics in both GDL are approximated by a coarse 3-section spatial discretization of the GDL. The channel mass balance ODEs in each electrode are added to the GDL subsystem, leading to a 24-state numeric model of ordinary differential-difference equations (full numeric model).

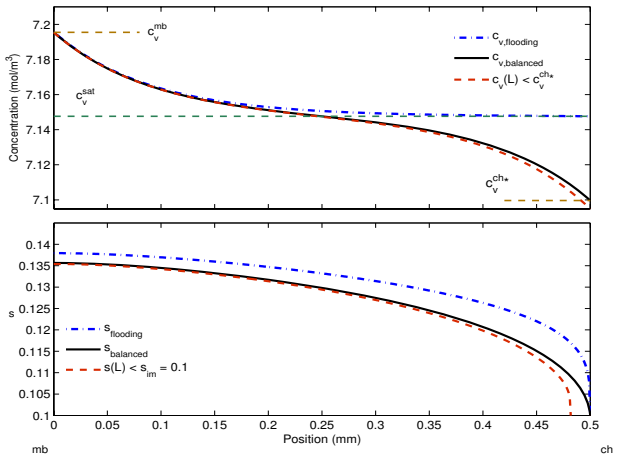

Figure 2. ANODE DISTRIBUTION OF LIQUID WATER RATIO FOR VARYING CHANNEL WATER VAPOR CONCENTRATIONS.

In the SAS, a combination of the quasi steady-state analytic solutions for the gas constituents $(c_{H_2}(x), c_{O_2}(x), c_{v,an}(x), c_{v,ca}(x))$ with the water saturation $(s(x,t))$ numeric differential algebraic equation (DAE) is created. Within the SAS, there is a further reduction since the amount of liquid water present in the cathode GDL does not influence the anode water distributions (as long as $s_{ca} > 0$). We therefore propose both 10-state and 7-state reduced models.

A C/O analysis will determine whether it is mathematically possible to control the GDL channel BC to obtain (17), which is critical for stabilization of the system. If the channel water mass can be controlled to a constant value, then the GDL liquid distribution will be stable ([1]). Further, it will be shown that if the channel liquid water mass can be brought to zero, controllability of the GDL liquid modes will be obtained. Additionally, this study will indicate the input(s) best-suited to obtain this control objective and the output(s) required.

Linearization of both the numeric 24-state model, and the reduced order SAS models (10-state and 7-state), allows generation of a state-space model form and use of C/O measures,

$$\dot{x} = Ax + Bu \quad y = Cx + Du.$$

Since the analysis is based upon a linearized system of switching nonlinear equations, the local C/O for three scenarios will be considered; $s(L,t) < s_{im}$ (receding front), $s(L,t) = s_{im}$ (borderline non-flooding), and for net liquid flow into the channel (flooding with $s(L,t) > s_{im}$).

4.1 Choice of Controllability-Observability Test

A number of C/O tests exist, ranging from the simple C/O matrix rank tests to computation of the respective grammians to determine if they are positive definite.

In spite of the removal of many of the fast (GDL) states, the fast channel states remain, and thus the stiff system characteristics of our model lead to an unavoidably (short of time-scaling)

large condition number. Unit scaling was performed to reduce the condition number, but even the minimum condition number (κ_{min}), represented by

$$\kappa_{min} = \frac{\lambda_i^{max}}{\lambda_i^{min}}, \text{ with } \kappa \triangleq \frac{\sigma_i^{max}}{\sigma_i^{min}}, \tag{32}$$

where σ and λ are the singular values and eigenvalues of the linearized system matrix A, is on the order of 10^6. Condition numbers of this magnitude are cause for concern, possibly causing large magnification of errors under matrix inversion due to computer rounding or modeling error.

The basic C/O matrix rank analysis tests will be avoided here due to their reliance on interpretation of the rank of matrices. A large condition number makes interpretation of rank subjective, as a decision must be made regarding C/O based on singular value relative magnitudes even though those values may on the order of 10^{30}. Further, the rank test does not provide information on which modes of the system are controllable/observable.

The Popov-Belevitch-Hautus (PBH) eigenvalue test has the benefit of being able of identifying C/O for each mode, because the controllability test is simply,

$$\text{rank}[\lambda_i I - A \quad B] = n \quad \forall\, \lambda_i \in \mathcal{C},$$

where each eigenvalue is tested and full rank indicates controllability. The observability requirement of a mode uses,

$$\text{rank} \begin{bmatrix} \lambda_i I - A \\ C \end{bmatrix} = n \quad \forall\, \lambda_i \in \mathcal{C}.$$

The PBH eigenvalue method still requires rank determination of a matrix with high condition number.

The PBH eigenvector test, on the other hand, provides a simple means to associate modes and their relative controllability, yet does not require a matrix rank evaluation. The concept behind the PBH eigenvector tests is based on considering the input and output matrices as operators that map the modes of the system to another space. If that space is the null space, then that mode is uncontrollable or unobservable or both, depending upon whether the input or output matrix was used in the test. Taken from [6], these test can be represented by:

$\bar{q}A = \lambda\bar{q}$ where $\bar{q}$ is a LH (row) eigenvector of A,

from which $\bar{q}B$=0 implies $\bar{q}$ is an uncontrollable mode. Similarly,

$A\bar{v} = \lambda\bar{v}$ where $\bar{v}$ is a RH (column) eigenvector of A,

and $C\bar{v}$=0 implies $\bar{v}$ is an unobservable mode.

This mapping results in a scalar value for each mode against each input or output vector in the matrices B and C. Further, the magnitude of the scalar value can be interpreted as an indication of the relative C/O of the mode versus a specific input/output.

It is demonstrated that the degree of coupling is affected by the operating point. For example, with the inputs described in Sec. 4.2, greater controllability of the liquid water modes is obtained when the channel condition is sub-saturated than when it is saturated. On the other hand, during anode flooding (which is associated with channel vapor saturation), the GDL anode liquid water becomes uncontrollable, yet observability is gained using cell voltage output.

4.2 About Control Inputs and Outputs

The possible control inputs for our system are related to channel constituent flow rates. In practice, both anode and cathode inlet streams can be humidified, though it is typical in our experiments to set the cathode inlet at 100% and the anode inlet at nearly 0% relative humidity, respectively. For this study, the general case of actuation via variably humidified inlet stream is assumed for both electrodes.

Typical implementation methods for the reactant flow rates include pressure control and flow control. In flow control, the upstream pressure is held constant, and a valve opening position is determined to provide the desired flow rate into the channel,

$$W^{in} = u_{flow} \cdot k^{in}(p_{source} - p^{ch}), \tag{33}$$

where $u_{flow} \in [0,1]$ is the position of the upstream valve, p^{ch} is the total pressure in the channel, p_{source} is the pressure upstream of the channel inlet, and k^{in} is an experimentally determined linear nozzle coefficient. In pressure control, the channel pressure is controlled via an outlet valve opening,

$$W^{out} = \bar{u} \cdot k^{out}\left(p^{ch} - p^{amb}\right), \tag{34}$$

where $\bar{u} \in [0,1]$ is the position of the downstream valve, P^{amb} is the ambient pressure, and k^{out} is another experimentally determined linear nozzle coefficient.

Since the end result in both cases can be related to reactant excess ratios λ_{H_2} and λ_{O_2}, to maintain generality these will be the final inputs considered in the analysis. The input function is,

$$u = g(RH_{an}^{in}, RH_{ca}^{in}, \lambda_{H_2}, \lambda_{O_2}). \tag{35}$$

In line with the goal of establishing a model for anode water control, the focus is on the anode channel inputs. The cathode side inputs of oxygen excess ratio and inlet humidity are included in the analysis, but it is shown that they have little effect on controllability outside the O_2 and N_2 distributions. Further, the λ_{O_2} input is commonly used for fuel cell power control and O_2 starvation prevention, suggesting that it would be prudent to leave the cathode inputs out of the anode side water control discussion.

In this work 12 cases are studied, combining variations in operating point and degree of model order reduction. Table 1 lists the key cases considered (each condition from column one is tested for each model of column 2). The reduced state models are included in the analysis to confirm that model reduction has not adversely affected the C/O. Additionally, for the 10-state model, 4 more tests combining the two practically available outputs were compared. The voltage output, based on a voltage degradation prediction model ([2]), and measurement of relative humidity (ϕ) in the channel were compared for flooding and borderline cases. The point is to determine the effect on observability for each of these outputs alone, and together. The voltage model enables the greatest range of observable states, due to its dependence upon liquid water in the anode channel, concentrations of oxygen, hydrogen, water vapor at the membrane, stack current, and temperature (as shown in [2]),

$$v_{cell} = f(m^{ch}_{w,an}, c^{mb}_{van}, c^{mb}_{v,ca}, c^{mb}_{H_2}, c^{mb}_{O_2}, I_{st}, T_{st}), \quad (36)$$

whereas relative humidity is only a function of water vapor concentration and temperature,

$$\phi = f(c^{ch}_{v,an}, T_{st}). \quad (37)$$

Table 1. CONTROLLABILITY/OBSERVABILITY CASES STUDIED

Condition	Model	
Flooding	24-state	Full numeric model
Borderline	10-state	SAS model (6 GDL + 4 channel states)
$s[3] < s_{im}$	7-state	SAS model (3 GDL + 4 channel states)

4.3 Surrogate States for Reduced Models

Residualization of the fast states by analytic solution to form algebraic equations has an influence on the state matrices of the fuel cell model. For example, in the full numeric 24-state model, the water vapor was a dynamic state in each spatially-discretized section. Upon implementation of the analytic solution for $c_{v,an}(x,t)$, the water vapor dynamic states are removed, and the analytic solution is inserted into dynamic state equations for $s_{an}(x,t)$. Given identical operating conditions, the SAS reduced model has very different state equations, as shown by (38)-(40). Residualization of the fast states has transferred the contributions of the gas states in the full numeric model to the remaining dynamic states in the reduced-order model that determine their analytic solutions. These surrogate states are the boundary conditions for the analytic solutions implemented.

When reducing the full numeric system to a reduced-order system under non-flooding conditions, with I_{st} = 75A, T_{st} = 333K, RH^{in}_{an} = 0, λ_{H_2} = 196%, and voltage output, the linearized output matrix C is altered:

$$\begin{aligned} C_{full} = {} & 0.747 c_{v,an}[1] + 0.747 c_{v,ca}[1] \\ & + 0.493 c_{H_2}[1] + 20.9 c_{O_2}[1], \end{aligned} \quad (38)$$

$$C_{red} = 0.492 c^{ch}_{H_2} + 20.3 c^{ch}_{O_2} + 0.024 m^{ch}_{w,an}. \quad (39)$$

Using as an example the liquid saturation nearest the channel, the state equations also change,

$$\begin{aligned} \dot{s}_{an}[3]_{full} &= 0.11 s_{an}[2] - 0.13 s_{an}[3] + 0.016 c_{v,an}[3], \\ \dot{s}_{an}[3]_{red} &= 0.08 s_{an}[2] - 0.04 s_{an}[3] + 0.02 m^{ch}_{w,an}. \end{aligned} \quad (40)$$

The hydrogen, oxygen, and anode vapor contributions have been related to their channel BC through the analytic solution, and are represented by the associated channel states. The generation of water at the membrane and high humidification of the cathode inlet stream leads to a condition of constant flooding and supersaturation in the cathode GDL. With the removal of the dynamic water vapor states, the cathode GDL water vapor distribution is influenced only through the membrane by the anode water vapor distribution. In the full numeric model, membrane water content is a function of the humidities in both anode and cathode at $x = 0$. However, with the removal of water vapor states, Table 2 shows that the water vapor concentration membrane gradient becomes only a function of anode channel water vapor.

Table 2. OUTPUT MATRIX SURROGATE STATES

Removed State	Surrogate State
$c_{v,ca}(x,t)$	$m^{ch}_{w,an}$
$c_{v,an}(x,t)$	$m^{ch}_{w,an}$
$c_{O_2}(x,t)$	$c^{ch}_{O_2}$
$c_{H_2}(x,t)$	$c^{ch}_{H_2}$

4.4 Controllability-Observability Results

Of foremost concern is that all the unstable modes are controllable and observable. In [5] it was shown that the liquid water states within the GDL are stable under any reasonable range of conditions if the channel water mass state is bounded, yet the channel liquid water mass can experience unbounded growth from bounded inputs. This anode channel instability leads to voltage degradation in the short term, and will cause fuel cell shut down if not addressed.

The results of the PBH eigenvector tests for the various model cases and condition sets are shown in Tables 3 and 4. In the table headings, the number refers to the number of states in the model (24 is the full numeric model). The letter (in the observability table) indicates the output used (Voltage and/or Humidity of anode channel). The modes column references mode groupings of states. Due to the nature of the difference-equation generated modes and the model, states of the same class (H_2 concentration, anode liquid water, etc.) tend to form modes together.

The C/O tests for the various cases result in the following conclusions (from data shown in Tables 3, 4):

1. Under flooding conditions (non-zero liquid water in the channel), the mass of water in the anode channel is a controllable mode, and can thus be steered back to zero with the anode inputs (light blue shading in Table 3).
2. The anode GDL liquid water modes are controllable under all non-flooding conditions (pink shading in Table 3).
3. During flooding, the water vapor (yellow shading in Table 3) and liquid water states in the anode GDL are uncontrollable. Under this condition, small changes in anode inlet/outlet flow do not influence water vapor concentration in the channel, thus blocking influence on GDL liquid states.
4. Observability of anode liquid water, on the other hand, improves with flooding conditions as the liquid water is seen

Table 3. CONTROLLABILITY PBH EIGENVECTOR TEST RESULT

	Flooding			Borderline			$s_{an}[3] < s_{im}$		
Mode	**24**	**10**	**7**	**24**	**10**	**7**	**24**	**10**	**7**
s_{an}	0	0	0	0.07	0.07	0.07	0.08	0.07	0.07
s_{an}	0	0	0	0.03	0.04	0.03	0.01	0.01	0.01
s_{an}	0	0	0	2e-3	9e-4	7e-4	0.01	0.01	0.01
s_{ca}	0	0	–	0	0	–	0	0	–
s_{ca}	0	0	–	0	0	–	0	0	–
s_{ca}	0	0	–	0	0	–	0	0	–
$m^{ch}_{w,an}$	0.043	0.089	0.089	12.0	11.9	11.9	12.2	11.6	11.9
c^{ch}_{an}	18.3	19.4	19.4	15.4	16.9	16.9	10.5	16.8	16.8
c^{ch}_{ca}	28.0	21.3	21.3	28.0	21.3	21.3	28.0	21.3	21.3
c^{ch}_{ca}	3.36	3.60	3.60	3.36	3.60	3.60	3.36	3.60	3.60
$m^{ch}_{w,ca}$	12.7	–	–	12.7	–	–	12.7	–	–
c_{H_2}	5.90	–	–	6.07	–	–	6.80	–	–
c_{H_2}	8.82	–	–	9.24	–	–	9.20	–	–
c_{H_2}	5.03	–	–	6.03	–	–	3.30	–	–
$c_{v,an}$	0	–	–	1.03	–	–	2.74	–	–
$c_{v,an}$	0	–	–	1.83	–	–	6.06	–	–
$c_{v,an}$	0	–	–	0.98	–	–	0.36	–	–
c_{O_2}	3.79	–	–	3.79	–	–	3.58	–	–
c_{O_2}	6.60	–	–	6.60	–	–	6.60	–	–
c_{O_2}	2.10	–	–	2.10	–	–	2.10	–	–
$c_{v,ca}$	0	–	–	0.34	–	–	0	–	–
$c_{v,ca}$	0	–	–	1.03	–	–	1.86	–	–
$c_{v,ca}$	0	–	–	1.36	–	–	2.27	–	–
c_{N_2}	6.28	–	–	6.28	–	–	6.27	–	–
Markers to key results (summarized below)									

Table 4. OBSERVABILITY PBH EIGENVECTOR TEST RESULT

	Flooding					Borderline				$s_{an}[3]<s_{im}$	
Mode	**24V**	**10V**	**10H**	**10VH**	**7V**	**24V**	**10V**	**10H**	**10VH**	**24V**	**10V**
s_{an}	1.09	1.09	0	1.09	1.09	0	0	0	0	0	0
s_{an}	0.48	0.48	0	0.48	0.48	0	0	0	0	0	0
s_{an}	0.17	0.16	0	0.16	0.16	0	0	0	0	0	0
s_{ca}	0	0	0	0	–	0	0	0	0	0	0
s_{ca}	0	0	0	0	–	0	0	0	0	0	0
s_{ca}	0	0	0	0	–	0	0	0	0	0	0
$m^{ch}_{w,an}$	2.34	2.34	0	2.34	2.34	0.30	0.29	0.56	0.63	0.30	0.29
c^{ch}_{an}	0.41	0.49	0	0.49	0.46	0.62	0.46	0.23	0.52	0.61	0.46
c^{ch}_{ca}	14.7	18.1	0	18.1	18.1	14.7	18.1	0	18.1	14.7	18.1
c^{ch}_{ca}	5.64	8.49	0	8.49	8.49	5.64	8.50	0	8.50	5.64	8.50
$m^{ch}_{w,ca}$	0	–	–	–	–	0	–	–	–	0	–
c_{H_2}	0.76	–	–	–	–	0.77	–	–	–	0.78	–
c_{H_2}	0.55	–	–	–	–	0.54	–	–	–	0.54	–
c_{H_2}	0.17	–	–	–	–	0.17	–	–	–	0.14	–
$c_{v,an}$	1.22	–	–	–	–	1.16	–	–	–	1.52	–
$c_{v,an}$	0.40	–	–	–	–	0.52	–	–	–	1.14	–
$c_{v,an}$	0.13	–	–	–	–	0.16	–	–	–	0.42	–
c_{O_2}	29.5	–	–	–	–	29.5	–	–	–	29.5	–
c_{O_2}	23.4	–	–	–	–	23.4	–	–	–	23.4	–
c_{O_2}	7.26	–	–	–	–	7.26	–	–	–	7.26	–
$c_{v,ca}$	1.67	–	–	–	–	1.50	–	–	–	0.27	–
$c_{v,ca}$	0.42	–	–	–	–	0.42	–	–	–	0.27	–
$c_{v,ca}$	0.04	–	–	–	–	0.17	–	–	–	0	–
c_{N_2}	6.85	–	–	–	–	6.85	–	–	–	6.85	–
Markers to key results (summarized below)											

in the degradation of the voltage due to liquid buildup in the channel (pink shading in Table 4).

5. GDL liquid water is only observable under flooding conditions, and then only in the anode. Cathode liquid water (GDL and channel) is unobservable under all conditions due to the decoupling of vapor and liquid under the assumption of a saturated cathode channel.
6. The number of observable mode increases significantly with use of voltage output versus use of relative humidity alone due to the many states contributing to the voltage estimation.
7. Use of relative humidity output alone results in unobservable anode channel modes during flooding (yellow shading in Table 4).
8. Combination of both outputs does not increase the number of modes that are observable due to output state redundancy, however observability of the anode channel modes improves when both outputs are used (light blue shading in Table 4).
9. When gaseous states in the GDL are reduced to algebraic equations, those voltage output matrix states are transformed to the channel concentrations via the analytic solutions (38).

The significance of the above results can be summarized:

1. Though GDL liquid modes are not controllable under flooding, stabilization of the anode water dynamics is possible since the unstable anode channel water mass is controllable.
2. The unobservable anode channel water mass when ϕ is the only output during flooding implies that though the water mass can be driven to zero, the controller will will not have any information on when the mass will be eliminated. If integral control is used, wind-up will be a concern. A combination of cell voltage and relative humidity outputs would alleviate this issue by making the water mass observable. Each of these two outputs provide important information lacking in the other; voltage output informs the controller that actuation is needed, and ϕ has information regarding whether drying or flooding is causing the voltage loss.
3. Together with channel liquid controllability above, controllability of the GDL liquid modes under all non-flooding conditions implies that the GDL liquid distribution can be shaped by the proposed inputs.
4. As $s[n]$ nearest the channel falls below the immobile saturation, controllability of liquid modes declines due to the buffer caused by the non-equilibrium condition in section *n*.

5 CONCLUSIONS

The liquid distribution within the GDL is controllable during non-flooding channel conditions, implying that practical fuel cell inputs can be effectively used to prevent flooding throughout the fuel cell. Further, the channel water mass is controllable even under flooding conditions though the mass is predominantly in liquid form. Again under flooding conditions, the combination of voltage and channel humidity outputs renders the channel water mass observable, thus state feedback to stabilize the channel

water is feasible. Use of channel humidity as the sole output is of questionable value as the channel water mass is not observable, at least in the linear model case, during flooding conditions.

REFERENCES

[1] McCain, B. A., Stefanopoulou, A. G., and Kolmanovsky, I. V., 2007. "A multi-component spatially-distributed model of two-phase flow for estimation and control of fuel cell water dynamics". 46th IEEE Conf. on Decision and Control CDC2007-1455.

[2] McKay, D. A., Siegel, J. B., Ott, W. T., and Stefanopoulou, A. G., 2008. "Parameterization and prediction of temporal fuel cell voltage behavior during flooding and drying conditions". *J. Power Sources,* **178**(1), pp. 207–222.

[3] McCain, B. A., Stefanopoulou, A. G., and Kolmanovsky, I. V. "A dynamic semi-analytic channel-to-channel model of two-phase water distribution for estimation and control of fuel cells". *Accepted IEEE Trans. in Control Systems Technology*.

[4] Nam, J. H., and Kaviany, M., 2003. "Effective diffusivity and water-saturation distribution in single- and two-layer PEMFC diffusion medium". *Int. J Heat Mass Transfer,* **46**, pp. 4595–4611.

[5] McCain, B. A., Stefanopoulou, A. G., and Kolmanovsky, I. V. "On the dynamics and control of through-plane water distributions in PEM fuel cells". *Chemical Engineering Science, doi: 10.1016/j.ces.2008.05.025*.

[6] Kailath, T., 1980. *Linear Systems*, 1st ed. Prentice Hall, Inc., Englewood Cliffs, NJ.

6 APPENDIX

Examples show that the linearized 24-state model accurately reflects the nonlinear system response to small input variations from equilibrium. Table 5 lists the key equilibrium values. In order to obtain linearization models, only the hydrogen stoichiometry was varied due to its strong influence on anode channel water mass (i.e. water vapor concentration).

Table 5. EQUILIBRIUM CONDITIONS FOR LINEARIZATION.

Condition	H_2 Stoich	I_{st} [A]	O_2 Stoich	Temp [K]
Borderline	2.02	75	3.0	333
Flooding	1.90	75	3.0	333
Drying	2.06	75	3.0	333

In this application, a coarse spatial discretization of the GDL into three sections was performed. Sec. 1 is closest to the membrane for anode and cathode, and sec. 3 is next to the channel.

The top subplots of Figs. 3-4 show s, the time-varying water saturation, for applicable sections of the GDL (typical values are between 0.11 and 0.16). The middle subplots show the water vapor concentration for the channel and each section.

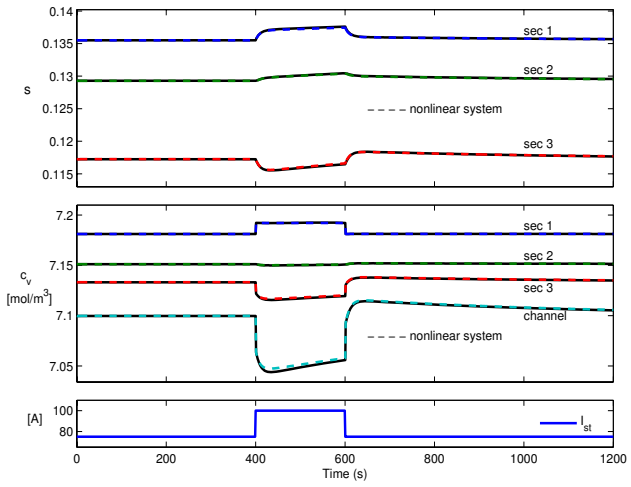

Figure 3. BORDERLINE CASE: LINEAR SYSTEM TRACKS NONLINEAR SYSTEM FOR A STACK CURRENT STEP UP/DOWN OF 25A.

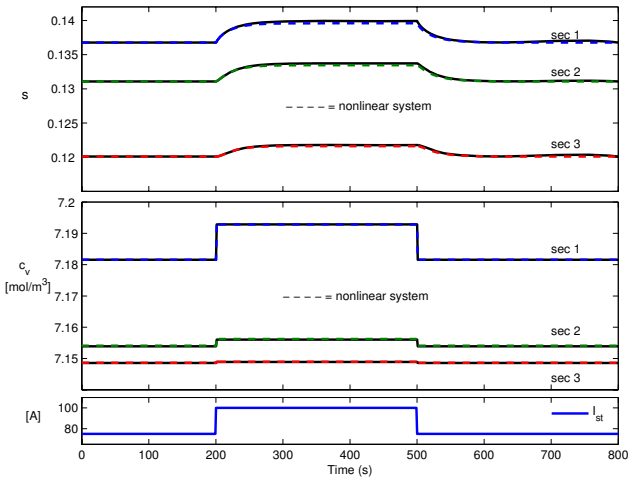

Figure 4. FLOODING CASE: LINEAR SYSTEM TRACKS NONLINEAR SYSTEM FOR A STACK CURRENT STEP UP/DOWN OF 25A.

Finally, the bottom subplots show the stepped input stack current. With changes in I_{st}, both s and c_v respond due to the dependence of anode flow rate and water production on stack current. For borderline and drying (not shown) cases, responses of sections near the channel are opposite to I_{st} changes, while sections near the membrane move in phase with I_{st}. However, under the flooding case, all sections are positively correlated to I_{st}. As can be seen from Figs. 3-4, the linearizations match the nonlinear system responses well for I_{st} steps up/down. Though not shown here, significantly larger input steps than those of Figs. 3-4 will result in notable response error (i.e. effect of nonlinearities).